Contact Angle, Film, and Line Tension of Foam Films. I. Stationary and Dynamic Contact Angle Measurements

I. B. IVANOV,[1] A. S. DIMITROV, A. D. NIKOLOV, N. D. DENKOV AND P. A. KRALCHEVSKY

Laboratory of Thermodynamics and Physico-Chemical Hydrodynamics, University of Sofia, Faculty of Chemistry, Sofia 1126, Bulgaria

Received February 20, 1991; accepted November 26, 1991

It is established experimentally that slowly shrinking small air bubbles attached to a liquid–air interface form a nonequilibrium (dynamic) contact angle. Aqueous solutions of sodium dodecyl sulfate (SDS) are used at two different concentrations of added electrolyte. A black thin liquid film is formed at the top of the bubble. The experimental cell used allows measurements with shrinking and expanding bubbles as well as with bubbles of constant equatorial radius. Hysteresis of the contact angle was observed. The results show that the shrinking of the contact line (advancing meniscus) causes deviation of the contact angle from its equilibrium value. The reliability of some previous work interpreting the change in contact angle with the radius of shrinking bubbles as a line tension effect is discussed.

1. INTRODUCTION

The present interest for line tension is related to its influence on the equilibrium at the three-phase contact line and, in particular, on the value of the contact angles (1, 2, 3). The theoretical studies revealed that similar to the surface tension, which is due to the excess of the free energy density in the narrow transition zone between two bulk phases (4, 5), the line tension is an excess of the surface tension in the transition zone around the three-phase contact line (6–9). Hence, the line tension is a second-order excess quantity and should play a role only for very small radii of the contact line. This is probably the source of the variety of experimental values for line tension determined by different authors: both positive and negative values, which differ sometimes by several orders of magnitude, have been reported.

Line tension has also been estimated by numerous theoretical calculations. A micromechanical theory of the line tension at the periphery of symmetric thin films was developed (10, 11). It demonstrates that the value of line tension is determined both by the changes of the interfacial tensions and by the local deviations of the interfacial profile in the transition region. The equations describing the profile of the transition region were extended in (12, 13) to arbitrarily shaped interfaces. According to the study of Evans (14), the bending energy can also contribute to line tension in the case of membrane-covered droplets. The possibility of measuring line tension from the shape of a liquid meniscus wetting a stripwise heterogeneous wall was also discussed (15, 16).

It is interesting to note that the theoretical studies predict systematically lower line tension values than those determined experimentally. For example, Starov and Churaev (17, 18) predicted theoretically a line tension $\kappa \approx 0.1$ nN for two attached emulsion droplets. With a similar emulsion system Wallace and Schurch (20) measured $\kappa = 10$–24 nN. Recent measurements with microscopic liquid lenses floating on a foam film provided an upper limit of about 10 nN for the magnitude of κ in this system (21). For the case of a solid–

[1] To whom correspondence should be addressed.

0021-9797/92 $5.00

liquid–vapor three phase contact line Tarazona and Navascues (7) found theoretically κ to vary between -0.026 and -0.082 nN. On the other hand, for systems of the same type, Neumann and coworkers (22, 23) measured positive values of κ, all being of the order of 1000 nN.

These discrepancies do not necessarily mean a failure of the theory or of the experiment. The theoretical values of line tension are probably correct, at least in order of magnitude, within the framework of the accepted simplified theoretical model. However, the real experimental situation might be much more complicated: a variety of unexpected or unaccounted effects could contribute to the measured line tension values. A more detailed investigation of a simple experimental system can help clarify the physical explanations for the large line tensions measured.

Such a relatively simple experimental system is a shrinking air bubble attached to a liquid–air interface. Platikanov *et al.* (36) detected experimentally changes in the contact angle with the shrinking of the contact line and attributed this effect to the action of line tension, κ. To calculate κ from the contact angle data these authors hypothesized that both the film and line tensions, γ and κ, are constant during bubble shrinkage and thus obtained values of κ of the order of 0.1 nN, both positive and negative. (Note that the equilibrium theory of de Feijter and Vrij (10) predicts $\kappa \sim -0.001$ nN for Newton black films.)

Later on in Ref. (24) we studied the same system as Platikanov *et al.* (36). However, instead of assuming constancy of γ and κ, we experimentally determined these two quantities during the process of bubble shrinkage. Our experiments (24) yielded line tension values varying with the radius of the contact line and having magnitudes of up to 100 nN for the largest bubbles. We also observed significant variations with the bubble radius of the film tension, γ, of the black foam film formed at the top of the bubble. The careful verification of the experimental procedure (25, 26) confirmed the reliability of our values of κ and γ (see also Section 4 below).

The data obtained in Ref. (24) were criticized and the experiment was qualified by some authors as "not correct" (27), "erroneous" (28), and "apparently erroneous" (29). This criticism was based essentially on the fact that in the experiments of Platikanov *et al.* (30, 27) for bubbles fixed at the tip of a capillary, the measured values of the film tension were independent of the curvature of the *film.* For discussion of some other arguments raised in Refs. 27 and 28 against our paper (24), the reader is referred to Ref. 31. However, a closer inspection reveals that the results of the two experiments, (24) and (30), are not only compatible (31), but they even support each other—see Section 4.

We believe that the only correct way to find the reason for the large line tensions measured in (24), is to study directly the role of various factors on the contact angle, film, and line tensions of *shrinking bubbles.* The first step in this direction was to exchange the anionic surfactant (SDS), which stabilizes the thin films, with a nonionic surfactant (32). The experiments with this system gave zero line tension.

The aim of the present study is to investigate the possible role of some nonequilibrium (dynamic) effects such as the motion of the contact line. Already in Ref. 24 we argued that the line tension values measured by the shrinking bubble method might be due, at least in part, to nonequilibrium effects. Such an effect, namely, the possible difference in surface tension between the meniscus and bubble surfaces, was then assumed and discussed. However, since at that time we did not dispose of a technique for controlling the rate of bubble shrinkage, it was not possible to discuss another effect also mentioned in Ref. 24—the motion of the three-phase contact line. Hence, we preferred to report in Ref. 24 our experimental data and their verification without going into speculations about the nature of the observed phenomena. In the present paper we report the results, obtained with a new ex-

perimental cell that allows measurements with bubbles of diminishing, expanding, and fixed equatorial radii (for the sake of brevity we call the latter "stopped bubbles"). The calculation of the film and line tensions requires interferometric measurement of the film curvature. Since this procedure is very delicate and time consuming we used it only in a few cases and the results are reported in Ref. (26). However, only measurements of the contact angle α (between the film and the meniscus) can give valuable information, bringing us closer to the answer to the problem of whether the observed effects are of equilibrium or nonequilibrium origin.

The next section is devoted primarily to the description of the new experimental cell. In Section 3 the experimental procedure and results are outlined. The conclusions, summarized in Section 4, reveal that the effects observed by us in Ref. (24) have nonequilibrium origin. The same is probably true for the results of Platikanov *et al.* (Refs. (36, 37)), who claim, however, to have measured equilibrium line tension. In an attempt to resolve the controversy on this subject existing in the literature, we analyzed also, based on our new findings, the experimental approaches used by Platikanov and co-workers.

2. EXPERIMENTAL SET UP AND MATERIALS

A scheme of the new experimental cell is presented in Fig. 1. The cylindrical holder, 1, and the two screw covers, 2 and 3, are made of Teflon. The upper and the bottom plates, 4 and 5, are optically plane-parallel glasses. Two plastic rings, 6 and 7, placed between the glass plates and the holder, provide hermetic isolation of the cell interior from the outer air. The pressure inside the cell can be controlled through the orifice, 8, which is connected with an aspiring pump by means of Teflon tubing. In our experiment we used a water jet pump.

A cylindrical glass vessel (of diameter 1.2 cm and height 1.3 cm) containing the surfactant solution is placed at the center of the cell.

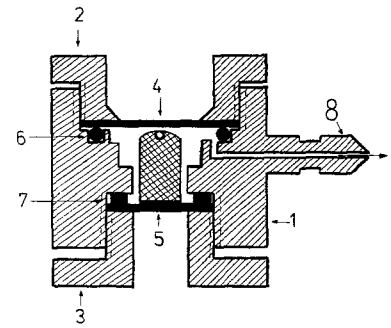

FIG. 1. Experimental cell of variable pressure—cross-section. (1) teflon holder, (2) and (3) screw covers, (4) and (5) optical glass plates, (6) and (7) isolation rings, (8) connection with the pump.

A slightly convex meniscus was formed so that a small floating bubble could be fixed at the center of the solution–air interface. At the beginning of each experiment the upper screw cover was open and a bubble of suitable size was blown out of a glass syringe. Then the cell was closed to allow saturation of the vapors above the solution. The connection between the cell and the pump passes through a glass container partially filled with water. Thus saturation of the water vapors in the hoses is also ensured. The pressure adjustment is done by a special screw valve of fine pitch. In addition, a petcock controls the connection of the system with the pump or, alternatively, with the atmosphere. In this way the pressure in the cell can be decreased or made equal to atmospheric.

Before each experiment the Teflon parts of the cell were cleaned by putting them into chromic acid and washing them afterwards with distilled water. The two optical glass plates, the central cylindrical glass vessel, and the glass syringe were kept for several hours in fresh chromic acid and then washed and rinsed with distilled water for 30 min.

The optical measurements were carried out with a microscope Epival Interphako (Carl Zeiss, Jena). The bubble was observed from above, through the optical glass plate. That is why we could not use microscope objectives

of too-short focusing distance like the objective (×25) used in our previous experiments (24). All of our measurements were carried out with objectives of ×10 and ×12.5. The construction of the microscope and the cell allows observation of the bubble both in reflected and transmitted light. Moreover, the microscope is specially designed for interferometric measurements (33, 34). The microscope is supplied with a photographic camera. In order to eliminate the vibrations the whole system with the microscope was mounted on top of a 4000 kg antivibrational block.

In order to be able to compare the new data with those from Ref. (24) we carried out the experiments with the same solutions as previously used: 0.05% (1.73×10^{-3} mol/liter) aqueous solutions of sodium dodecyl sulfate (Fluka BioChemika) at two concentrations of NaCl (Merk, analytical grade, heated for 5 h at 400°C): 0.25 and 0.32 mol/liter. The solutions were prepared with water of surface tension 72.4 mN/m obtained from Milli-Q water purification system. The experiments were carried out in a thermostated room at 22 ± 0.5°C. The surface tension of the two solutions used (with 0.25 and 0.32 mol/liter NaCl) were 32.4 and 31.7 mN/m, respectively.

3. EXPERIMENTAL PROCEDURE AND RESULTS

The experimental cell shown in Fig. 1 allows measurements with (i) shrinking bubbles, (ii) expanding bubbles, and (iii) stopped bubbles. They are considered separately below.

(i) Shrinking Bubble

This method was first used by Princen and Mason (35) for studying film permeability to gases and then in Refs. (24, 32, 36, 37) for investigation of the contact angle and line tension of foam films. With the new cell we applied the method in the following way.

At the beginning an air bubble of initial radius about 400 μm is formed by means of the glass syringe. Then the cell is closed hermetically by means of the upper screw cover.

A thin foam film intervenes between the air inside and outside the bubble—Fig. 2. Due to the higher pressure inside the bubble there is a gas diffusion flux across the film. As a result the bubble shrinks with time.

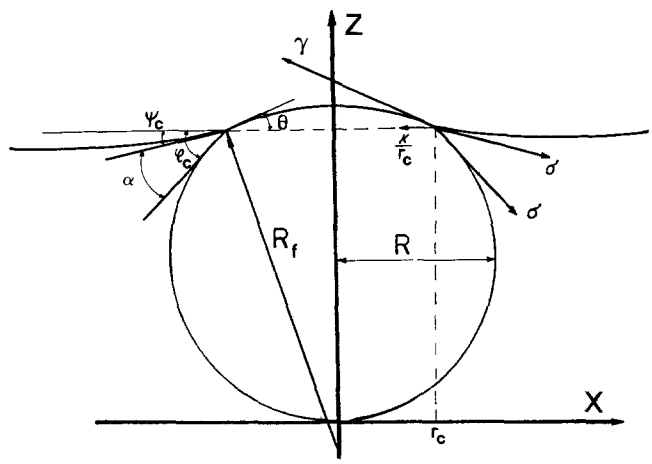

FIG. 2. Cross-section of an air bubble attached to a liquid–air interface. r_c, R, and R_f are the radii of the contact line, bubble equator, and film curvature, respectively; γ, σ, and κ are the film, surface, and line tensions, respectively.

At the beginning the size of the bubble is larger than the observation field of the microscope. One and a half hours after the formation of the bubble it becomes small enough (equatorial radius $R < 300$ μm) and the measurements can be started. The contact line radius r_c (Fig. 2) is measured in reflected light (illumination through the microscope objective). The equatorial bubble radius R is measured in transmitted light. To increase the accuracy the values of r_c and R were recorded visually at the moment when the diameter of the respective circumference was equal to an integer number of scale divisions. The dependencies of R and r_c on time t are fitted by means of smooth curves as explained in Ref. (24)—see Fig. 3. The contact radius r_c can be measured directly due to the fact that in our case the film is extremely thin, the contact angle is large, and the contact line is sharp. For example Lyklema and Mysels (38, 39) measured values of h less than 10 nm for SDS solutions with electrolyte concentration larger than 0.2 mol/liter. The respective contact angle α is larger than 13°. According to Babak (40) the uncertainty in the visual determination of r_c, Δr_c, is of the order of $h/\tan(\alpha/2)$. With the above values of h and α, one calculates $\Delta r_c < 0.08$ μm, which is less than the experimental precision of measurement of r_c—about 0.3 μm. In his estimate Babak used $h = 100$ nm, $\alpha \approx 0.2°$, and obtained $\Delta r_c = 50$ μm. Since the latter values of h and α are very different from the real thickness and contact angle in our experiments, the estimate of Babak (40) does not apply to our measurements. (A special procedure for determining r_c was developed in Ref. (32) for the case of small ($\sim 1°$) contact angles.)

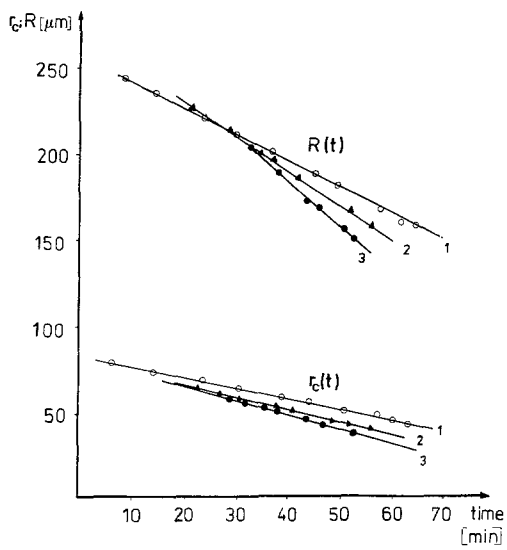

FIG. 3. Experimental data for the dependence of the equatorial and contact line radii, R and r_c, on time t for three consecutive shrinkings of the same bubble at atmospheric pressure (the solution with 0.25 mol/liter NaCl).

The spontaneous diminishing of the bubble accelerates with time. Finally the bubble shrinks virtually into a point and disappears. However, the experimental cell in Fig. 1 enables one to prevent the disappearance of the bubble and to investigate several spontaneous shrinkages of the same bubble. This is achieved in the following way.

When the equatorial radius R of a shrinking bubble decreases to about 150 μm one can lower the pressure inside the cell by using the water jet pump. This leads to an increase of the bubble volume. Indeed, in accordance with the ideal gas law, $V = \text{const}/P_b$, the bubble volume V is inversely proportional to the bubble pressure P_b. When the equatorial radius, R, of the expanding bubble reached 300 μm we closed the screw valve and thus we fixed a new lower value of the pressure inside the cell. In spite of that, the bubble size kept increasing with time. This is probably due to the slow desorbtion of gas, whose concentration in the solution is higher than the equilibrium one, corresponding to the newly established lower pressure. After waiting 20–30 min (the bubble slowly expands during this period) we increased the pressure up to atmospheric and then kept it constant. As a result the bubble shrank to 200–230 μm and then it continued to shrink spontaneously. Measurements of R and r_c were periodically carried out again.

When R reached 150 μm the bubble was expanded again and the procedure was repeated.

Figure 3 presents data for R and r_c measured during three consecutive spontaneous shrinkings of the same bubble at atmospheric pressure. The numbering of the curves corresponds to the sequence of shrinkings. Curves 1 in Fig. 3 represent R and r_c for the first spontaneous shrinking of a bubble formed in a 0.05% SDS solution with 0.25 mol/liter NaCl. At the moment when R = 150 μm the bubble was expanded as described above. Curves 2 and 3 correspond to the second and third spontaneous shrinking of the same bubble. One sees that the slope of a curve increases with its number; i.e., with each consecutive expansion the rate of shrinking increases. This is probably due to the fact that after the atmospheric pressure has been quickly restored inside the cell, the solution remains undersaturated with air, which makes it possible for the air to escape from the bubble not only through the film, but also through the air–solution interface.

Curves 0–1 and 2–3 in Fig. 4 represent the values of the contact angle α, calculated from data for $R(t)$ and $r_c(t)$ shown in Fig. 3. More precisely, curve 0–1 corresponds to the first spontaneous shrinking of the bubble (curves 1 in Fig. 3), whereas the values of α for the next two shrinkings of the same bubble (curves 2 and 3 in Fig. 3) lie on the same curve 2–3. The contact angle for curve 2–3 is pronouncedly smaller compared with that of the first shrinking (curve 0–1). The values of α were calculated from the measured R and r_c by using the procedure described in Section 3 of Ref. (24). The only difference is that instead of using the asymptotic formula [11] in (24) we integrated numerically the Laplace equation to determine φ_c. (The asymptotic formula in Ref. (24) is accurate enough for the relatively small bubbles investigated in Ref. (24).) The method of numerical integration of the Laplace equation for the bubble surface is similar to the method used in Ref. (32).

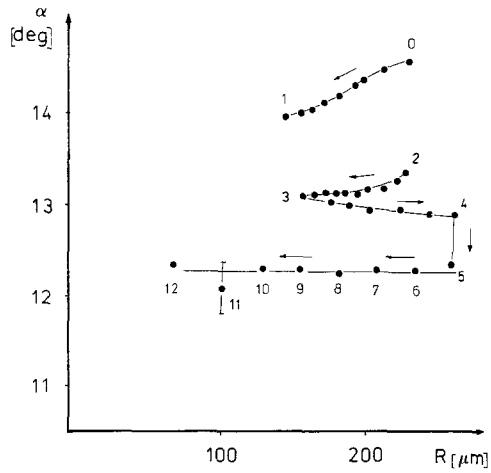

FIG. 4. Values of the contact angle α of one and the same bubble at different conditions: 0–1 and 2–3, spontaneous shrinkings; 3–4, gradual expansion; 4–5, relaxation at fixed R; 5, 6, . . . , 12, equilibrium values of α for different fixed R.

(ii) Gradually Expanding Bubble

The cell depicted in Fig. 1 allows also experiments with *expanding* rather than shrinking bubbles. A bubble can be made to expand by suitably controlling the pressure decrease through the screw valve. The procedure for measurements of R and r_c, as well as the computation of the contact angle α, are the same as for shrinking bubbles. The rate of expansion in our experiments was from 2 to 10 times higher than the rate of spontaneous shrinking. Curve 3–4 in Fig. 4 illustrates the typical behavior of the contact angle α during the expansion of a bubble. When R came down to 150 μm (Point 3) the bubble was gradually expanded up to R = 260 μm (Point 4) with a mean velocity of $dr_c/dt \approx 4$ μm/min. Curve 3–4 shows that the contact angle α for this process exhibits a slight decrease with time.

(iii) Stopped Bubble

The spontaneous diminishing of the bubble radius R can be stopped when the shrinking due to the escaping of gas from the bubble is exactly compensated by a suitable decrease of the pressure inside the experimental cell. The

process of spontaneous shrinking is relatively slow for not-too-small bubbles: $dR/dt \approx 0.25$ μm/s at $R = 200$ μm and $dR/dt \approx 0.40$ μm/s at $R = 80$ μm. So it turned out to be possible to keep R constant within ± 5 μm by manual adjustment of the pressure by means of the fine screw valve accompanied by simultaneous observations of the equatorial bubble diameter.

The observation showed that in spite of the constancy of R, the contact line radius r_c and thereby the contact angle α keep decreasing with time (see curve 4–5 in Fig. 4). The values of the contact angle α as a function of time for two solutions are presented in Fig. 5. One observes a typical relaxation behavior: α decreases with time until some equilibrium value α_e of α is reached. The relaxation is more pronounced for the solution containing less electrolyte (the one with 0.25 mol/liter NaCl). The relaxation time (determined from the slope of the plot ln δ vs t—not shown) is $t_r = 50$ min for curve 1 in Fig. 5 (0.25 mol/liter), whereas $t_r = 130$ min for curve 2 (0.32 mol/liter). The radii of these bubbles were $R \sim 280$ μm.

Let us return now to Fig. 4. After the relaxation 4–5 (at constant R), the bubble was allowed again to shrink from $R = 260$ μm to $R = 230$ μm (from point 5 to point 6) and then it was stopped again and allowed to relax. The *equilibrium* values, α_e, of α in points 5 and 6 turned out to coincide within the experimental accuracy. This procedure was repeated several times: all the transitions from 5–6 up to 11–12 correspond to shrinking, whereas the values of α in points 5, 6, . . . , 12 are the equilibrium contact angles reached after the relaxation. This experiment shows that the *equilibrium* value α_e of the contact angle does not depend on the bubble size in the investigated region of radii. We call α_e "equilibrium" angle because it was reached during a process of relaxation. However, we are aware of the fact that the "stopped" bubble is not in a state of full thermodynamic equilibrium, even after the contact angle has fully relaxed. Indeed, the pressure drop and the gas diffusion flux across the thin liquid film still exist.

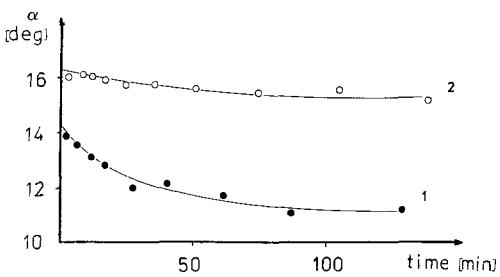

FIG. 5. Relaxation of the contact angle α with time t for stopped bubbles of radius $R = 280$ μm: (●) 0.25 mol/liter NaCl; (○) 0.32 mol/liter NaCl.

It is interesting to note that, whereas the first relaxation 4–5 took 30 min, the next relaxations were considerably faster: the relaxation in point 10 needed 8 min and the relaxation in point 12 took only 1 min. So a tendency of the time for relaxation to decrease with R is observed.

Additional information about the dynamic behavior of the contact angle of small bubbles is provided by the experimental data presented in Fig. 6. In Fig. 6a the data for α are plotted versus the bubble radius R, whereas in Fig. 6b the same data are presented as a function of time.

Curve 0–1 corresponds to an initial spontaneous shrinking of the bubble at atmospheric pressure. At $R = 150$ μm the process of shrinking was stopped as described above. The contact angle of the stopped bubble decreased from 13.5° to the equilibrium value $\alpha_e = 12.2°$. The relaxation process 1–2 took 30 min. (If the bubble had not been stopped, it would have shrunk from $R = 150$ μm to $R = 0$ during 40 min.) The relaxed bubble was then gradually expanded from $R = 150$ μm to $R = 220$ μm with a mean rate of $dR/dt \approx 2.5$ μm/min. It is important to note that no changes in the contact angle were observed during this process of expansion: $\alpha = \alpha_e$ on the segment 2–3 in Fig. 6. After the expansion, the bubble was allowed to shrink spontaneously again at constant pressure—curve 3–4. As seen in Fig.

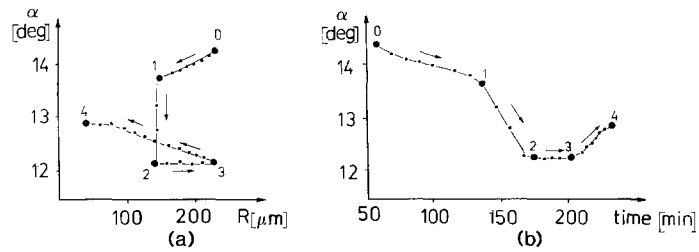

FIG. 6. The contact angle α of an air bubble as a function of the equatorial bubble radius R (a), and of time (b). 0–1-spontaneous shrinking; 1–2 relaxation at $R = 152$ μm; 2–3 gradual expansion; 3–4, spontaneous shrinking.

6, the shrinking was accompanied with an increase of the contact angle, which exhibits a tendency to level off at a value of about 13° for the small bubbles (Fig. 6a).

The comparison between the processes 2–3 and 3–4 shows that in the case of a receding meniscus (expanding contact line) the contact angle keeps its equilibrium value, whereas in the case of an advancing meniscus (shrinking contact line) the contact angle increasingly deviates from its equilibrium value. Such behavior is typical of hysteresis effects observed often with contact angles under dynamic conditions. In the case of smooth and homogeneous interfaces (as it is in our case) the hysteresis can be due to the interactions between the two meniscus surfaces (41).

Finally, let us compare segment 3–4 in Fig. 4 and segment 2–3 in Fig. 6, which both correspond to expansion. The difference between them is that the contact line expansion is carried out before (Fig. 4) and after (Fig. 6) the relaxation of the contact angle. Therefore, the decrease of α during the process 3–4 in Fig. 4 can be due to contact angle relaxation.

4. DISCUSSION

Let us summarize the main conclusions we reached, based on the experiments described above:

(i) There is pronounced difference between the contact angles measured during two consecutive spontaneous shrinkings realized with one and the same bubble–compare curves 0–1 and 2–3 in Fig. 4.

(ii) When the spontaneous shrinking of a bubble is stopped by fixing the equatorial radius R (i.e., the capillary pressure) a relaxation of the contact angle α is observed—see curve 1–2 in Fig. 6. During the relaxation α changes more than 1° for the investigated solutions.

(iii) If after the contact angle has relaxed the bubble is allowed to shrink spontaneously again, the contact angle deviates from its equilibrium value, α_e, and starts to increase—see curve 3–4 in Fig. 6. The latter fact implies that the shrinking of the contact line causes deviation of the contact angle from its equilibrium value.

The general conclusion we are led to by these experiments is that the contact angle of the spontaneously shrinking bubbles in the investigated solutions is a nonequilibrium one. It seems reasonable to assume that the nonequilibrium effects observed with the contact angle in the present paper and the surprising variations of the film and line tension with bubble size established in Ref. (24) with shrinking bubbles have common physical origin. The results presented and discussed in the second part of this study, Ref. (26) support this claim. Here we will only mention in advance that both the film and the line tension of a stopped bubble exhibit relaxation. Moreover, during the relaxation, the film tension approaches its equilibrium value (coinciding with the value measured by de Feijter (42) for

macroscopic films), whereas the line tension approaches zero.

Following the ideas developed in (41) one can hypothesize that the observed contact angle hysteresis is due to some short-range attractive surface forces counteracting the detachment of the film surfaces during the shrinking of the contact line. A theoretical model for describing this phenomenon is currently being developed.

As pointed out above, experiments with shrinking bubbles were performed also by Platikanov *et al.* (36, 37). However, since they did not measure the radius of curvature of the film R_f, they could not determine the film and line tensions independently. To make up for the missing experimental information these authors hypothesized that during the bubble shrinkage the film tension, γ, remained constant and equal to its equilibrium value. As a result of this hypothesis their calculated values of line tension, κ, are independent of the bubble radius and about two orders of magnitude smaller than the values of κ determined in our experiments (24) for the same system. The new results for the contact angle, presented in this paper, provide a basis for an analysis of the approach by Platikanov *et al.* (36, 37).

On the Diminishing Bubble Method

In their experiments with spontaneously shrinking bubbles Platikanov *et al.* (36, 37) measured only R and r_c (see Fig. 2), and then calculated the contact angle α. According to their results α levels off for large bubbles ($R > 70\ \mu$m), whereas a deviation of α from constancy was established with the smaller bubbles (see, e.g., Fig. 9 in Ref. (29)). The latter fact was interpreted as an effect of the line tension κ in accordance with the equation

$$\frac{1}{\cos \alpha/2} = \frac{2\sigma}{\gamma} - \frac{\kappa}{\gamma}\frac{1}{r_c}, \qquad [1]$$

where σ and γ are the surface tension of the solution and the film tension, respectively. Equation [1] is an approximated version of Eq. [60] in Ref. (9), which follows from the Neumann–Young force balance at the contact line. If γ and κ were constants, they could be determined from the slope and the intersect of the plot $1/\cos(\alpha/2)$ vs $1/r_c$, as Platikanov *et al.* did.

This approach for determining line tension, called the "diminishing bubble method," seems to be simple and convincing. Its weak point is the hypothesis that both γ and κ are constant during the bubble shrinking. The arguments of Platikanov *et al.* (29, 37, 43) in favor of this hypothesis are the following: (a) The contact angle α was found experimentally to level off for the large bubbles when the line tension effect should be negligible (hence γ = const at least with the larger bubbles—see Eq. [1]). (b) Independent experiments (27, 30) with curved foam films formed at the tip of a capillary showed that the film tension γ was constant over a wide range of R_f (70–700 μm). (c) The line tension κ determined by means of the "diminishing bubble" method agrees by its sign and order of magnitude with the results for κ obtained by two other methods developed by Platikanov *et al.*: The "critical bubble" method (44) and the "porous plate" method (43, 45).

As a matter of fact the present study, as well as our previous work (24, 26), allows checking experimentally the hypothesis in question. With respect to argument (a), the constancy of α for the larger bubbles established in (29, 37) turned out to be an artifact. It is due to the systematic error introduced by the approximated formula (Eq. [7] in Ref. (37)), which was used in Refs. (29, 37) for calculation of α from the data for r_c and R. By rigorous computer integration of the Laplace equation for the shape of the bubble surface we recalculated the correct values of the contact angle by using the data from curve 1 in Fig. 9 in (29). The results are compared in Fig. 7 with the curve of Platikanov *et al.* (29). It is clear that the correct values of α (filled circles) do not level off at large R and that the systematic error of the approximated formula

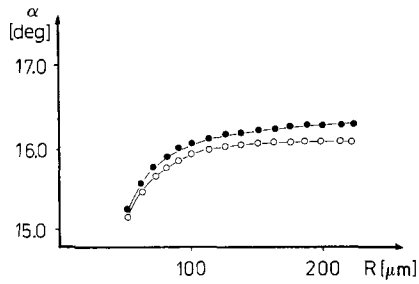

FIG. 7. Contact angle α vs bubble radius R: data by Platikanov *et al.* (37) processed by means of their approximated formula (○) and by rigirous integration of the Laplace equation (●).

increases with R; in particular, $\Delta\alpha \approx 0.34°$ at $R = 200\ \mu m$.

Our data for α vs R (see Figs. 4 and 6) also do not exhibit a tendency for leveling off at large R. Besides, the dependence of α on R turns out to depend on the evolution of the bubble before the start of the measurements—cf. curves 0–1 and 2–3 in Fig. 4. Moreover, the fact that the contact angle α of a stopped bubble relaxes (curve 1–2 in Fig. 6) and that α changes when a relaxed bubble is allowed to shrink again (curve 3–4 in Fig. 6) clearly demonstrates that the contact angle α of a shrinking bubble is a nonequilibrium one. Then the dependence of α on r_c, observed by Platikanov *et al.* (36, 37) can well be a nonequilibrium effect (similar to the relaxation shown in Fig. 5) rather than being due to an equilibrium line tension as argued by Platikanov *et al.* In addition, the independent measurements of γ and κ in Refs. (24, 26) show that $\cos(\alpha/2)$ is almost a constant, whereas γ and κ undergo large variations with r_c (i.e., the plot of $1/\cos(\alpha/2)$ vs $1/r_c$ cannot be used for determining κ) see Fig. 8 in Ref. (24).

As far as the measurement of the film tension γ of films fixed on the tip of a capillary (27, 30) is concerned, in this case Platikanov *et al.* obviously deal with a motionless (nonshrinking) contact line. As our experiments demonstrated in such a case both α (see Fig. 5) and γ (Figs. 9, 10, and 11 in Ref. (26)) relax with time and eventually reach equilibrium values. Hence the experiment with bubbles fixed on a capillary cannot serve as proof that γ is constant also for shrinking bubbles. This conclusion is in line with the observation by Platikanov *et al.* (Ref. (30) p. 75) that measurements done immediately after the film formation yield larger (according to us—nonequilibrium) values of γ. In addition, it is established in Part II of this study, Ref. (26), that after the relaxation of the contact angle is completed, the film tension becomes equal to the equilibrium value measured by de Feijter (42), just like the film tension measured in (30). Therefore, our results in Ref. (24) are not in contradiction with those in Ref. (30) as claimed in Refs. (27, 28, 29).

The third argument of Platikanov *et al.* (29, 43) against our data is based on the agreement (by order of magnitude) between the results obtained by them by means of the diminishing bubble method and the so-called critical bubble and porous plate methods (44, 45). This could have been a strong argument if the last two methods were irreproachable, which unfortunately is not the case. Hence, we discuss below briefly some problems connected with the interpretation of the experimental data obtained by these methods.

On the Critical Bubble Method

In Ref. (44) the attachment of small bubbles at the surface of SDS aqueous solutions was studied. It was established that under certain conditions only the larger bubbles (with $R > R_{cr}$) formed black foam films, while the smaller ones (with $R < R_{cr}$) remained beneath the surface touching it but not forming a visible three-phase contact line. The smallest bubble forming a three-phase contact line was called "the critical bubble" and its radius was denoted by R_{cr}.

The following apparently simple explanation of this phenomenon has been proposed (44). An equivalent form of Eq. [1] reads

$$\gamma + \frac{\kappa}{r_c}\cos\frac{\alpha}{2} = 2\sigma\cos\frac{\alpha}{2}. \qquad [2]$$

The maximum value of the right-hand side of Eq. [2] is 2σ at $\alpha = 0$, while the left-hand side can grow infinitely as $r_c \to 0$ (if κ is not zero). So, it was hypothesized in (44) that (a) the critical bubble has a contact radius r_{cr} such that at $r_c < R_{cr}$ the equilibrium condition [2] is violated and (b) the contact angle α of the critical bubble is zero. Thus by setting $\alpha = 0$ in Eq. [2] one obtains

$$\kappa = (2\sigma - \gamma)r_{cr}. \qquad [3]$$

r_{cr} was determined in the following way (44). The small bubbles are almost spherical; then $r_{cr} \approx R_{cr}\sin\varphi_c = R_{cr}\sin\psi_c$ (α is supposed to be zero with the critical bubble)—cf. Fig. 2. Besides, the buoyancy force is counterbalanced by the meniscus surface tension:

$$\frac{4}{3}\pi R_{cr}^3\rho g = 2\pi r_{cr}\sigma\sin\psi_c.$$

The elimination of $\sin\psi_c$ yields

$$r_{cr}^2 = \frac{2\rho g}{3\sigma}R_{cr}^4, \qquad [4]$$

and from Eq. [3] one obtains the basic formula of the critical bubble method,

$$\kappa = (2\sigma - \gamma)\sqrt{\frac{2\rho g}{3\sigma}}R_{cr}^2. \qquad [5]$$

The main problems with the use of Eq. [5] for the interpretation of the experimental data are the following:

(i) If the "critical" behavior of the bubble is due to the breakdown of Eq. [1], applied by the authors (see Refs. (36, 37)) to shrinking bubbles, it is not clear why a large spontaneously shrinking bubble (like the bubbles studied both in the present study and in (24, 36)) does not exhibit any critical behavior at $R = R_{cr}$. The experimental dependence of r_c on R for such a bubble (data from Run 2b in Ref. (24) 0.32 mol/liter NaCl) is depicted with a solid line in Fig. 8. It is obvious that the condition for mechanical equilibrium, Eq. [2], is satisfied both for $R > R_{cr}$ and for $R < R_{cr}$.

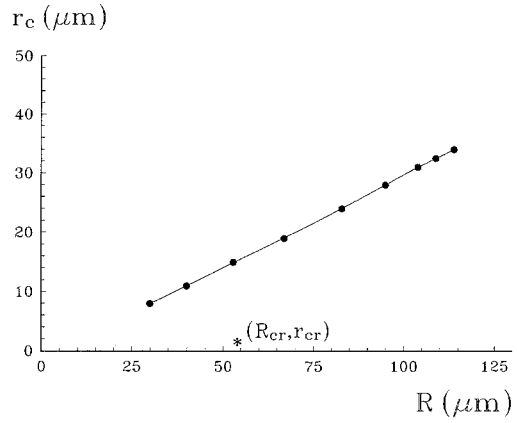

FIG. 8. Experimental data for r_c vs R for a spontaneously shrinking bubble (0.32 mol/liter NaCl). The asterisk denotes the position of the "critical" point, calculated from Eq. [4] with R_{cr} = 54 μm measured in (43, 44) for the same solution.

(ii) In Ref. (51) R_{cr} = 54 μm was determined for the solution with 0.32 mol/liter NaCl. Following the reasoning of the authors of Ref. 51, their critical bubble radius R_{cr} should correspond to a critical film radius, r_{cr}, which could be calculated from Eq. [4]. In this way we obtained for this system r_{cr} = 1.3 μm. The corresponding point (R_{cr}, r_{cr}) is shown in Fig. 8. The fact that it is situated far away from the equilibrium curve r_c vs R casts doubt on the applicability to this phenomenon of Eqs. [2]–[4], which all have equilibrium nature. In this connection it is worthwhile noting that Babak (40) proposed an alternative (and we believe plausible) interpretation of the data for the critical bubbles, based on kinetic considerations, without making use of any line tension effect.

(iii) In order for Eq. [5] to be used it is assumed (43) that the isolated point (R_{cr}, r_{cr}) corresponds to a metastable equilibrium state that is not specified. Quite arbitrarily it is supposed implicitly that this state corresponds to a Newton black film and the value of γ measured by de Feijter (42) for macroscopic Newton black films can be used. If the nonattached

bubbles (with $R < R_{cr}$) form "submicroscopic films," as stated in (44), it seems to us that it is better to substitute the film tension of these thicker films for γ in Eq. [5]. Say, for electrostatically stabilized films, $\theta_\infty \approx 1°$ ($\gamma = 2\sigma \cos \theta_\infty$)—see, e.g., (42). Then Eq. [5] gives $\kappa = 8 \times 10^{-7}$ dyn, which is about 100 times smaller than the value obtained in Ref. 43 by using Newton black film tensions.

(iv) In (44, 46) the barrier preventing the smaller bubbles (with $R < R_{cr}$) to form film is interpreted as a line tension effect by means of some force consideration, which seems to be applicable for solid, rather than for fluid, particles—cf. p. 614 in (44). Since these considerations in fact do not affect Eq. [5], we will not analyze them here.

In summary, not only the line tension value calculated from Eq. [5], but also the very concept for the existence of a line tension barrier preventing thin film formation, is problematic and needs both theoretical and experimental justification.

On the Porous Plate Method

The porous plate method was introduced by Mysels and Jones (47), who studied experimentally the dependence of the thin film interactions on the film thickness. Zorin *et al.* (45) applied this method for line tension measurements in accordance with the Neumann–Young equation,

$$\gamma + \frac{\kappa}{r_c} = 2\sigma \cos \theta_0, \qquad [6]$$

where $\theta_0 = \alpha/2$ is half of the contact angle. If the formed flat foam films are at an equilibrium state, and if the slight dependence of γ on r_c (due to the dependence of γ on the capillary pressure) can be neglected, then in keeping with Eq. [6] any observed dependence of θ_0 on r_c can be attributed to the line tension effect. To measure θ_0 Zorin *et al.* (45) used two independent approaches: (i) capillary pressure measurements and (ii) interferometric measurements. These two approaches are discussed separately below.

(i) Capillary pressure measurements. A simple integration of the Laplace equation $d(x \sin \theta)/(xdx) = P_c/\sigma$ for $r_c < x < R$ yields (48, 52)

$$P_c = 2\sigma \frac{R \cos \theta_R - r_c \sin \theta_0}{R^2 - r_c^2}. \qquad [7]$$

Here R is the radius of the vertical cylindrical hole in the porous plate supporting the film and θ_R is the contact angle subtended between the surface of the liquid meniscus and the inner surface of the hole. (In the case of perfect wetting, θ_R must be zero.) Zorin *et al.* measured the quantity,

$$\Delta P = P_c - \frac{2\sigma}{R} \cos \theta_R \qquad [8]$$

and plotted the data versus the contact radius r_c. This experimental curve was compared in their Fig. 2 with the theoretical curve ΔP vs r_c calculated from Eqs. [7] and [8] at constant θ_0 (no line tension effect). A slight difference between this theoretical and the experimental curve was interpreted as a line tension effect. However, Zorin *et al.* did not publish any error estimates of ΔP and r_c, which is desirable when measuring a small effect such as κ.

To get an idea about the accuracy of these measurements we used the equation:

$$\frac{\Delta P}{2\sigma} r_c \left[\left(\frac{R}{r_c} \right)^3 - \frac{R}{r_c} \right] = \cos \theta_R - \frac{R}{r_c} \sin \theta_0, \qquad [9]$$

which follows directly from Eqs. [7] and [8]. Then we took the data for ΔP and r_c from the table in Ref. (45) and plotted the left-hand side of Eq. [9] (denoted by F) vs R/r_c—see Fig. 9. (The data are for a 0.05% aqueous solution of SDS with 0.32 mol/liter NaCl, $T = 21°C$, $\sigma = 31.8$ mN/m, $R = 120$ μm.) The data fit a straight line with a correlation coefficient of 0.9991. The slope yields $\theta_0 = 7.85° \pm 0.11°$, which is markedly lower than the results of the interferometric measurement of the same authors giving θ_0 as varying between 8.23° and 9.30° (45). The intersect yields θ_R

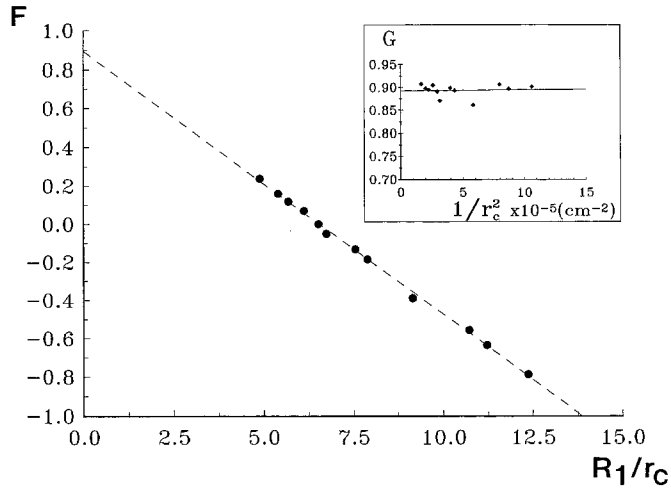

FIG. 9. The left-hand side of Eq. [9] plotted vs R/r_c: data are from the Table in Ref. (45). $F = (\Delta P/2\sigma)r_c[(R/r_c)^3 - (R/r_c)]$. The inset shows the plot of the left-hand side of Eq. [11] vs $1/r_c^2$. $G = F + (R/r_c)\sin\theta_\infty$.

$= 26.6° \pm 2.0°$. This high value of θ_R seems to be unrealistic because the glass porous plate soaked with the solution must be well wettable.

In the plot of F vs R/r_c shown in Fig. 9 there are no visible deviations from the straight line suggesting the presence of a line tension effect on θ_0. For a closer inspection of this point from Eq. [6] we determined $\sin\theta_0$:

$$\sin\theta_0 = \left[1 - \frac{\gamma^2}{4\sigma^2}\left(1 + \frac{\kappa}{\gamma r_c}\right)^2\right]^{1/2}.$$

Since $\kappa/\gamma r_c \ll 1$, one obtains

$$\sin\theta_0 = \sin\theta_\infty\left(1 - \frac{2\kappa}{\gamma r_c}\cot^2\theta_\infty\right)^{1/2}, \quad [10]$$

where θ_∞ is the limiting value of θ_0 for large r_c: $\cos\theta_\infty = \gamma/2\sigma$—cf. Eq. [6]. If $\kappa \approx 10^{-10}$ N (as claimed in Ref. 45) and $\theta_\infty \approx 8°$, then the square root in Eq. [10] can be expanded in series. We substituted the resulting expression for $\sin\theta_0$ in Eq. [9] to obtain

$$\frac{\Delta P}{2\sigma} r_c\left[\left(\frac{R}{r_c}\right)^3 - \frac{R}{r_c}\right] + \frac{R}{r_c}\sin\theta_\infty = \cos\theta_R + \frac{\kappa R}{\gamma}\frac{\cos^2\theta_\infty}{\sin\theta_\infty}\frac{1}{r_c^2}. \quad [11]$$

For θ_∞ we used the value 7.85° determined from the slope of the plot of F vs $1/r_c$. In the inset of Fig. 9 the left-hand side of Eq. [11], denoted by G, is plotted against $1/r_c^2$. Having in mind Eq. [11], from the slope of the straight line we determined $\kappa = (0.8 \pm 5.5) \times 10^{-11}$ N. In other words, it turns out that κ is zero in the framework of the experimental accuracy.

In conclusion, we deem the capillary pressure measurements presented in (45) to be not reliable enough, especially for line tension measurements.

(ii) Interferometric measurements. Zorin *et al.* (45) applied transmitted light differential interferometry to determine the meniscus shape from the interference pattern and to calculate the contact angle θ_0 from the interference pattern. Then they plotted $(1 - \cos\theta_0)$ vs $1/r_c$ and fitted the data with a straight line—see Fig. 10. By using Eq. 6 from the slope of the straight line they calculated $\kappa = +3$ nN for 0.32 mol/liter NaCl and $\kappa = -1.5$ nN for 0.45 mol/liter NaCl. The intersects in Fig. 3 of Ref. (45) give $\theta_\infty = 10.12°$ for 0.32 mol/liter NaCl, while de Feijter (42) determined $\theta_\infty = 9.13°$ with the same con-

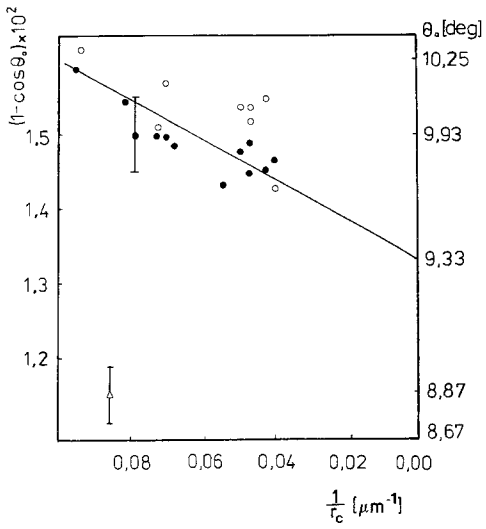

FIG. 10. Dependence of $(1 - \cos\theta_0)$ on $1/r_c$ as obtained by Zorin *et al.* (45) (0.45 mol/liter NaCl). The triangle is an experimental point, recalculated from the interference data in (45) by using the procedure developed in (21).

centrations of NaCl and SDS. With 0.45 mol/liter NaCl the respective values are $\theta_\infty = 9.33°$ for the data of Zorin *et al.* and $\theta_\infty = 11.26°$ for the data of de Feijter.

These considerable differences in θ_∞, which are not mentioned in Ref. (45), can be due to improper computer processing of the data for the interference fringes. To check this possibility we used the rigorous method for processing interferometric data developed in Ref. (21), which has been tested there both with model and experimental data. We processed the numerical data for the positions of the interference fringes, measured from a single photograph, which were presented as illustrative examples in Ref. (45). As a result we obtained $r_c = 11.8$ μm and $\theta_0 = 8.86°$. The respective point (denoted by a triangle in Fig. 10) turned out to be located away from the data of Zorin *et al.* If all other points are recalculated in the same way, one might expect a better agreement with de Feijter's value for θ_∞. However, it is not possible to predict how much the value of the line tension κ will change as a result of such a recalculation. It should be noted also that only the points denoted by open circles in Fig. 10 were obtained from the interferometric determination of θ_0. The filled circles were calculated by using the following special procedure. The quantity $R_0 = R/\cos\theta_R$ was determined by processing the interference pattern at a given moment. The result was substituted in the right-hand side of the equation

$$\sin\theta_0 = \frac{r_c}{R_0} + \frac{\Delta P}{2\sigma}\left(r_c - \frac{R_0^2}{r_c}\cos^2\theta_R\right), \quad [12]$$

which is equivalent to Eq. [9]. Then by using the independently measured ΔP (see above) and by setting $\theta_R = 0$ the angle θ_0 was calculated.

We believe that the agreement achieved in this way between the interferometric and capillary pressure measurements is fortuitous. Indeed, as shown above the data for ΔP are consistent with the values $\theta_0 = 7.85°$ and $\theta_R = 26.6°$, corresponding to the slope and the intersect in Fig. 9. If $\theta_R = 26.6°$ is used, it yields $R_0 = 107$ μm instead of $R_0 = 116$–120 μm obtained by the authors of Ref. (45) from the interferometric measurements. Therefore, the procedure used in (45) for calculation of the filled circles in Fig. 10 is not entirely self-consistent.

In summary, the line tension measurements with the porous plate method need further work. The points raised above lead us to the conclusion that neither the magnitude nor the sign of the line tension values obtained in Ref. (45) are totally reliable.

5. CONCLUDING REMARKS

The main result in the present paper is the experimental finding that slowly shrinking small air bubbles attached to a liquid–air interface form a *nonequilibrium* (dynamic) contact angle. The velocity of shrinkage of the contact line is really very small: $dr_c/dt \approx 9.2 \times 10^{-3}$ μm/s for a bubble of radius $R \approx 200$ μm. Nevertheless, this rate turns out to be large

enough to cause a noticeable deviation of the contact angle from its equilibrium value.

To study the dynamic behavior of the contact angle a specially designed experimental cell with variable pressure was constructed. It allows the shrinking of a bubble to be stopped and even to be reversed into an expansion. The contact angle of a stopped, initially shrinking bubble relaxes for about 1 h or more to reach its equilibrium value. The relaxation time depends on the radius of the bubble and electrolyte concentration for the investigated solutions of SDS. In addition, if a relaxed bubble is allowed to shrink again, the contact angle deviates from its equilibrium value—see Fig. 6. On the contrary, if a relaxed bubble is gradually expanded, no changes of the contact angle were noticed. These facts imply that the very shrinking of the contact line (corresponding to an advancing meniscus) causes the deviation of the contact angle from its equilibrium value.

The new data shed some light on the line tension measurements with shrinking bubbles. In particular, the change of the contact angle with the bubble radius, which was interpreted in Ref. (36) as a line tension effect can well be due to the observed nonequilibrium phenomena. This raises considerable doubt about the reliability of the line tension values reported in a number of publications (29, 36, 37, 46, 49, 50).

On the other hand, the new results suggest that the large line tension measured in Ref. (24), as well as the accompanying film tension variations, can be in fact nonequilibrium values of the respective quantities. This idea is supported experimentally in Ref. (26). It is established there that both the film and line tension of a stopped bubble (which previously had been shrinking) relax together with the contact angle.

ACKNOWLEDGMENT

The authors are indebted to Referee I for his valuable comments.

REFERENCES

1. Pethica, B. A., *Rep. Prog. Appl. Chem.* **46,** 41 (1961).
2. Pujado, P. R., and Scriven, L. E., *J. Colloid Interface Sci.* **40,** 82 (1972).
3. Pethica, B. A., *J. Colloid Interface Sci.* **62,** 567 (1977).
4. Ono, S., and Kondo, S., *in* "Handbuch der Physik," Vol. 10, Springer, Berlin, 1960.
5. Rowlinson, J. S., and Widom, B., "Molecular Theory of Capillarity," Clarendon, Oxford, 1982.
6. Buff, F. P., *J. Chem. Phys.* **26,** 23 (1957).
7. Tarazona, P., and Navascues, G., *J. Chem. Phys.* **75,** 3114 (1981).
8. Vignes-Adler, M., and Brenner, H., *J. Colloid Interface Sci.* **103,** 11 (1985).
9. Ivanov, I. B., Kralchevsky, P. A., and Nikolov, A. D., *J. Colloid Interface Sci.* **112,** 97 (1986).
10. de Feijter, J. A., and Vrij, A., *J. Electroanal. Chem.* **47,** 9 (1972).
11. Kralchevsky, P. A., and Ivanov, I. B., *Chem. Phys. Lett.* **121,** 116 (1985).
12. Ivanov, I. B., and Kralchevsky, P. A., *in* "Thin Liquid Films" (I. B. Ivanov, Ed.), p. 49. Dekker, New York, 1988.
13. Kralchevsky, P. A., and Ivanov, I. B., *J. Colloid Interface Sci.* **137,** 234 (1990).
14. Evans, E., *Colloids Surf.* **43,** 327 (1990).
15. Boruvka, L., Gaydos, J., and Neumann, A. W., *Colloids Surf.* **43,** 307 (1990).
16. Budziak, C. J., and Neumann, A. W., *Colloids Surf.* **43,** 279 (1990).
17. Starov, V. M., and Churaev, N. V., *Kolloidn. Zh.* **42,** 703 (1980).
18. Churaev, N. V., and Starov, V. M., *J. Colloid Interface Sci.* **103,** 301 (1985).
19. Torza, S., and Mason, S. G., *Kolloid. Z. Z. Polym.* **246,** 593 (1971).
20. Wallace, J. A., and Schurch, S., *J. Colloid Interface Sci.* **124,** 452 (1988).
21. Dimitrov, A. S., Kralchevsky, P. A., Nikolov, A. D., and Wasan, D. T., *Colloids Surf.* **47** (1990).
22. Gaydos, J., and Neumann, A. W., *J. Colloid Interface Sci.* **120,** 76 (1987).
23. Li, D., and Neumann, A. W., *Colloids Surf.* **43,** 195 (1990).
24. Kralchevsky, P. A., Nikolov, A. D., and Ivanov, I. B., *J. Colloid Interface Sci.* **112,** 132 (1986).
25. Nikolov, A. D., Dimitrov, A. S., and Kralchevsky, P. A., *Optica Acta* **33,** 1359 (1986).
26. Dimitrov, A. S., Nikolov, A. D., Kralchevsky, P. A., and Ivanov, I. B., *J. Colloid Interface Sci.* **151** (1992).
27. Platikanov, D., Nedyalkov, M., Scheludko, A., and Toshev, B. V., *J. Colloid Interface Sci.* **121,** 100 (1988).
28. Derjaguin, B. V., and Churaev, N. V., *J. Colloid Interface Sci.* **129,** 582 (1989).

29. Toshev, B. V., Platikanov, D., and Scheludko, A., *Langmuir* **4,** 489 (1988).
30. Platikanov, D., Nedyalkov, M., and Rangelova, N., *Colloid Polym. Sci.* **265,** 72 (1987).
31. Ivanov, I. B., Nikolov, A. D., Kralchevsky, P. A., and Denkov, N. D., *J. Colloid Interface Sci.* **134,** 294 (1990).
32. Lobo, L. A., Nikolov, A. D., Dimitrov, A. S., Kralchevsky, P. A., and Wasan, D. T., *Langmuir* **6,** 995 (1990).
33. Beyer, H., *Jenaer Rundsch.* **16,** 82 (1971).
34. Nikolov, A. D., Kralchevsky, P. A., and Ivanov, I. B., *J. Colloid Interface Sci.* **112,** 122 (1986).
35. Princen, H. M., and Mason, S. G., *J. Colloid Sci.* **20,** 353 (1965).
36. Platikanov, D., Nedyalkov, M., and Nasteva, V., *J. Colloid Interface Sci.* **75,** 620 (1980).
37. Nedyalkov, M., and Platikanov, D., Abhanlungen Akad., Wissensch. DDR, VI Intern. Tag. Grenzfl. Stoffe, Nr. 1N, p. 123, Akademie-Verlag, Berlin, 1985.
38. Lyklema, J., and Mysels, K. J., *J. Amer. Chem. Soc.* **87,** 2539 (1965).
39. Jones, M. N., Mysels, K. J., and Scholten, P. C., *Trans. Faraday Soc.* **62,** 1336 (1966).
40. Babak, V. G., *Colloids Surf.* **25,** 205 (1987).
41. Martynov, G. A., Starov, V. M., and Churaev, N. V., *Kolloidn. Zh.* **39,** 472 (1977).
42. de Feijter, J. A., Ph.D. Thesis. University of Utrecht, 1973; de Feijter, J. A., and Vrij, A., *J. Colloid Interface Sci.* **64,** 269 (1978).
43. Platikanov, D., Doctoral Thesis. University of Sofia, BG, 1989.
44. Platikanov, D., Nedyalkov, M., and Scheludko, A., *J. Colloid Interface Sci.* **75,** 612 (1980).
45. Zorin, Z. M., Platikanov, D., Rangelova, N., and Scheludko, A., *in* "Surface Forces and Interface Liquid Layers" (B. V. Derjaguin, Ed.) p. 200. Nauka, Moscow, 1983, in Russian.
46. Scheludko, A., Toshev, B. V., and Platikanov, D., *in* "The Modern Theory of Capillarity" (F. C. Goodrich and A. I. Rusanov, Eds.). Akademie-Verlag, Berlin, 1981.
47. Mysels, K. J., and Jones, M. N., *Disc. Faraday Soc.* **42,** 42 (1966).
48. Exerova, D., Ivanov, I. B., and Scheludko, A., *in* "Research in Surface Forces" (B. V. Derjaguin, Ed.), p. 144. National Bureau of Standards USA, Washington, DC, 1964.
49. Platikanov, D., and Nedyalkov, M., *in* "Microscopic Aspects of Adhesion and Lubrication" (J. M. Georges, Ed.) p. 97. Elsevier, Amsterdam, 1982.
50. Scheludko, A., "Colloid Chemistry," p. 261. Mir, Moscow, 1984. in Russian
51. Nedyalkov, M., and Platikanov, D., *Ann. Univ. Sofia, Fac. Chem.* **74,** 358 (1979/1980).
52. Toshev, B. V., and Ivanov, I. B., *Ann. Univ. Sofia, Fac. Chem.* **65,** 329 (1970/1971).